Amino Acids (2012) 43:1451–1464
DOI 10.1007/s00726-012-1218-x

ORIGINAL ARTICLE

Insilico study of the $A_{2A}R$–D_2R kinetics and interfacial contact surface for heteromerization

Amresh Prakash · Pratibha Mehta Luthra

Received: 12 August 2011 / Accepted: 4 January 2012 / Published online: 26 January 2012

Abstract G-protein-coupled receptors (GPCRs) are cell surface receptors. The dynamic property of receptor–receptor interactions in GPCRs modulates the kinetics of G-protein signaling and stability. In the present work, the structural and dynamic study of $A_{2A}R$–D_2R interactions was carried to acquire the understanding of the $A_{2A}R$–D_2R receptor activation and deactivation process, facilitating the design of novel drugs and therapeutic target for Parkinson's disease. The structure-based features (Alpha, Beta, SurfAlpha, and SurfBeta; GapIndex, Leakiness and Gap Volume) and slow mode model (ENM) facilitated the prediction of kinetics (K_{off}, K_{on}, and K_d) of $A_{2A}R$–D_2R interactions. The results demonstrated the correlation coefficient 0.294 for K_d and K_{on} and the correlation coefficient 0.635 for K_d and K_{off}, and indicated stable interfacial contacts in the formation of heterodimer. The coulombic interaction involving the C-terminal tails of the $A_{2A}R$ and intracellular loops (ICLs) of D_2R led to the formation of interfacial contacts between $A_{2A}R$–D_2R. The properties of structural dynamics, ENM and KFC server-based hot-spot analysis illustrated the stoichiometry of $A_{2A}R$–D_2R contact interfaces as dimer. The propensity of amino acid residues involved in $A_{2A}R$–D_2R interaction revealed the presence of positively (R, H and K) and negatively (E and D) charged structural motif of TMs and ICL3 of $A_{2A}R$ and D_2R at interface of dimer contact. Essentially, in silico structural and dynamic study of $A_{2A}R$–D_2R interactions will provide the basic understanding of the $A_{2A}R$–D_2R interfacial contact surface for activation and deactivation processes, and could be used as constructive model to recognize the protein–protein interactions in receptor assimilations.

Keywords $A_{2A}R$ · D_2R · Kinetic constant · Dimer · Parkinson's disease

Abbreviations

$A_{2A}R$	Adenosine A_{2A} receptor
ACE	Atomic contact energy
AD-ENM	Analysis of dynamics of elastic network model
ANM	Anisotropic network model
BRET	Bioluminescence resonance energy transfer
CVFF	Consistent valence force field
D_2R	Dopamine D_2 receptor
DSSP	Define secondary structure of proteins
ECLs	Extracellular loops
ENM	Elastic network model
FADE	Fast atomic density evaluator
FFT	Fast Fourier transform method
FRET	Fluorescence resonance energy transfer
GNM	Gaussian network model
GPCRs	G-protein-coupled receptors
ICLs	Intracellular loops
KFC	Knowledge-based FADE and contacts
MD	Molecular dynamics
MSF	Mean-squared fluctuation
NSAD	Normalized square atomic displacement
PD	Parkinson's disease
PMDB	Protein model database
PPI	Protein–protein interaction

Electronic supplementary material The online version of this article (doi:10.1007/s00726-012-1218-x) contains supplementary material, which is available to authorized users.

A. Prakash · P. M. Luthra (✉)
Medicinal Chemistry Division, Dr. B.R. Ambedkar Center for Biomedical Research, University of Delhi, North Campus, Mall Road, Delhi 110007, India
e-mail: pmlsci@yahoo.com; pmluthra@acbr.du.ac.in

PSC	Pairwise shape complementarities
SAVS	Structural analysis and verification server
SCR	Structurally conserved regions
SSM	Secondary structure matching
TM	Transmembrane

Introduction

The concept of G-protein-coupled receptor (GPCRs) oligomerization postulated that an intra-membrane neuropeptide and monoamine receptor–receptor interaction was responsible for the functional cross-talk observed between these two neurotransmitter systems (Agnati et al. 1980; Fuxe et al. 1983). This phenomenon is crucial for the receptor biosynthesis, maturation, trafficking, plasma membrane diffusion, pharmacology and signaling. Biophysical and biochemical approaches have revealed that GPCR signaling systems involve a succession of events that initially take place at the cell membrane and modulate the production and propagation of second-messenger molecules inside the cell (Lamb1996; Ferrandon et al. 2009).

The presence of $A_{2A}R$–D_2R heteromer was demonstrated in the striatal membrane preparations of brain (Ferre and Fuxe 1992; Ferre et al. 1993). Later, behavioral study and biochemical data showed that stimulation of $A_{2A}R$ inhibited and blockade potentiated a D_2R-mediated locomotor activation in mice, and that stimulation of D_2R counteracted on $A_{2A}R$-mediated cataleptic effect in rats (Fuxe et al. 2005). $A_{2A}R$ and D_2R are expressed in striatopallidal gamma-amino butyric acid neurons (GABAergic neurons) and their heterodimerization modulated the receptor functions in CNS (Agnati et al. 2003; Borroto-Escuela et al. 2010a, b). Adenosine inhibited dopamine-induced locomotor activity in the basal ganglia, mediated through $A_{2A}R$–D_2R heteromer contributing the fine-tuning of neural activity; however, exact mechanism is unclear. The presence of $A_{2A}R$ and D_2R in basal ganglia, a region of the brain that is involved in sensory-motor integration, incited these receptor–receptor interactions, and is an important target for PD therapy (Canals et al. 2003; Ciruela et al. 2006; Dalrymple et al. 2008).

FRET approach (Lohse et al. 2008; Vilardaga et al. 2009) revealed that intramolecular rearrangements associated with receptor activation in live cells proceed with fast kinetics (Vilardaga et al. 2003). The activation of a receptor by a small neurotransmitter such as the $A_{2A}R$, α_{2A} and β_1-adrenergic receptors (β_1R), and muscarinic receptors takes place with a time constant $\tau \approx 40$ ms, whereas activation of the receptor for the larger parathyroid hormone proceeds within $\tau \approx 1$ s (Vilardaga et al. 2003; Vilardaga 2010; Maier-Peuschel et al. 2010). Activated GPCRs then interact with heterotrimeric G proteins with kinetics that, in the context of the low level of G proteins, are not determined by the time course of receptor activation, but rather by a diffusion-limited collision process. FRET and BRET approaches have demonstrated the occurrence of $A_{2A}R$–D_2R hetrodimerization in a heterologous mammalian expression system (Canals et al. 2003; Soriano and Ventura 2009; Fuxe et al. 2010; Borroto-Escuela et al. 2010a, b). However, the stoichiometry of $A_{2A}R$–D_2R heteromers and the exact biophysical or molecular mechanisms of $A_{2A}R$–D_2R signaling to exert its physiological and pathological effects are yet to be revealed. Moreover, in the context of the low level of G proteins, the kinetics of GPCRs cannot be determined by the time course of receptor activation, thus limiting such studies in wet laboratory experiments (Vilardaga et al. 2010).

Several computerized modeling and pull-down mass spectrometry techniques have demonstrated the hetromerization between the $A_{2A}R$ and D_2R, and presumed that interface contacts were depended on the coulombic interaction between the D_2R–ICLs and C-terminal tails of the $A_{2A}R$ (Canals et al. 2003; Ferre et al. 2004; Ciruela et al. 2004; Woods et al. 2005). Conversely, the MD simulation of proteins to study the conformational changes at atomic level poses a formidable challenge to the process of molecular dynamics, and severely limits the method in both simulation time and system size. However, MD simulation provides an important insight about the changes in free energies with modulation in conformation with respect to time variance. The conformational mechanisms involved in biomolecular functions are determined by the intrinsic dynamics of biomolecules and define the overall structural architecture (Eisenmesser et al. 2005). The recognition of conformational dynamics at the atomic level is significant in protein functions including protein–ligand interactions, and allosteric regulation (Bahar et al. 2007; Henzler-Wildman and Kern 2007; Boehr et al. 2009).

First step toward understanding molecular mechanisms relevant to biological function involved an assessment of the propensity of amino acid residues at equilibrium dynamics of proteins, and the cooperative fluctuations accessible under native state conditions. For studying the equilibrium dynamics of proteins and capturing such slow cooperative fluctuations in native state conditions, NMA tool was developed (Brooks et al. 2004; Cui and Bahar 2005). In a typical NMA of protein dynamics, an atomic or coarse-grained potential function is approximated by a harmonic potential near a minimal-energy conformation, from which a Hessian matrix (the second derivatives of potential function) is calculated. A set of normal modes are solved from the Hessian matrix, which can be used to

describe small-amplitude atomic motions at low temperatures. Under harmonic assumption, the inverse of the eigenvalue of a normal mode is proportional to the MSF of atomic coordinates along the direction of its eigenvector. In recent years, ENMs including the anisotropic network model and its isotropic variation, the Gaussian network model have been developed to model protein dynamics at amino acid resolution (Yang et al. 2006; Eran et al. 2006). ENM can explicitly explain the protein association (k_{on})–dissiociation (k_{off}) processes, which are fundamental in understanding the protein–protein interaction (PPI). Building of quantitative models to predict kinetic constant based on kinetic process of PPI is necessitated for developing new theories or discovering new structure-based features related to PPI. Bai et al. (2011) calculated the 35 structure-based features (e.g., Alpha, Beta, SurfAlpha, and SurfBeta; GapIndex, Leakiness and Gap Volume) and their correlations with kinetic constants were analyzed. Subsets of these features were selected and used to build linear predictive models for K_{off}, K_{on}, and K_d which may facilitate the prediction of kinetic constant of PPI by structure-based properties.

Furthermore, the identification of the amino acid residues that is critical to determine the interfacial contacts, their regio-specificity and their mechanism of interaction will help to design the model for PPI. However, in the absence of detailed structural information, identification of the amino acid residues responsible for contact dimerization remains overwhelming challenge (Mustafi and Palczewski 2009). Furthermore, the crystal structure of majority of proteins is yet unknown, and 3D structure of protein is essential to understand how protein performs its function. Variety of advanced homology modeling methods have been developed which can efficiently provide reliable models of proteins. The predicted model of $A_{2A}R$ has explored thoroughly for understanding the antagonist–receptor interaction and improvising their properties as investigated in both pre- and post-$A_{2A}R$ crystal structure (Kim et al. 2003; Ivanov et al. 2007, 2009; Müller and Jacobson 2011). Jaakola et al. used T4-lysozyme (T4L) fusion strategy (Engel et al. 2002; Rosenbaum et al. 2007) to crystallize $A_{2A}R$, and most of the third cytoplasmic loop (L209–A221) residues were replaced with 160 amino acid residues of β_2R and T4L. Since the final refined crystal structure included residues from I_3 to Q_{310} of the human $A_{2A}R$ only, 3D structure of $A_{2A}R$ with loops was predicted using crystal and predicted structure of $A_{2A}R$ (Luthra et al. 2009; Mishra et al. 2010). The present work was carried to study the mechanisms of $A_{2A}R$ and D_2R hetromerization. Since BRET and FRET studies showed that the residues 375–405 belonging to C-terminals of $A_{2A}R$ were involved in $A_{2A}R$–D_2R heteromerization, the predicted structure of $A_{2A}R$ was used to carry the study.

The structure of $A_{2A}R$ and D_2R was predicted using the multiple template ($A_{2A}R$, β_2R and D_3R) approach. The role of ICLs, stoichiometry of contacts and the forces involved in interaction were elucidated with using ZDOCK, MD simulation. The propensity of amino acid residues involved in PPI was explicated with the execution of AD-ENM, GNM and H-bond perturbations. The kinetic profile of $A_{2A}R$–D_2R hetrodimerization was revealed with ENM process and validated. The kinetic profile assay of $A_{2A}R$–D_2R may provide the important clue to understand the pharmacology of receptors integration, and the structural roles of various residues involve in interfacial interaction.

Materials and methods

Molecular modeling of $A_{2A}R$ and D_2R with loops

The 3D models were constructed for $A_{2A}R$ and D_2R with ECLs and ICLs by means of homology modeling using recent version of MODELLER 9.9 (http://www.salilab.org/modeller/) with selecting multiple templates: β_2R (PDB ID: 2RH1; 2.40 Å), D_3R (PDB ID: 3PBL; 2.89 Å), $A_{2A}R$ (PDB ID: 3EML; 2.60 Å) and Modeled $A_{2A}R$ (PMBD: PM0074986). The primary sequence of $A_{2A}R$ (UniProt ID: P29274) and D_2R (UniProt ID: P14416) was obtained from Expasy server. The templates were aligned and SCRs were calculated. $A_{2A}R$ and D_2R amino acid sequence was aligned with template sequences using multiple sequence alignment tool Clustal-X (2.0.11) (Larkin et al. 2007). The coordinates were calculated for atoms that have equivalent atoms in the templates, and CHARMm internal coordinates were used for remaining unknown coordinates (Accelrys Inc. 2002). The initial modeled structures were further refined by MD simulation to achieve the convergence: 0.005 kcal mol^{-1} $Å^{-1}$ (Discover 3 User Guide 1999). The overall stereo-chemical quality of the $A_{2A}R$ and D_2R models was assessed on SAVS server (Laskoswki et al. 1993; Hooft et al. 1996). Finally, the 3D co-ordinates of optimized model were submitted to PMDB server (Castrignanò et al. 2005). The root mean square deviation between the main chain atoms of models and respective templates was calculated by structural superimpositions of predicted structures with their respective templates using PyMOL (DeLano 2003).

Protein–protein docking for heterodimer complex of $A_{2A}R$ with D_2R

The ZDOCKpro module of Insight II was used for protein–protein docking, consisting of two major components: ZDOCK and RDOCK. ZDOCK is a rigid-body, initial stage protein–protein docking algorithm that applies the

ligand rotation and the shape complementarity method through the FFT. The ZDOCK scoring function in this release was based on PSC. RDOCK is based on the CHARMm simulation program and was used for further refinement of poses generated by ZDOCK. It also ranks the docked structures based on the CHARMm electrostatic interaction energy and atomic contact energy (ACE) desolvation energy (Zhang et al. 1997).

To obtain the bound structures of $A_{2A}R$ with D_2R, the grid size was set to 128 Å × 128 Å × 128 Å grids, using a grid spacing of 1 Å. The total 54,000 poses of protein complex were calculated with angular step: 6° to get more accurate prediction. ZDOCK reports the predicted poses in the ZDOCK output file (ZOutput-File). These poses were sorted by ZDOCK_filter, i.e., PSC to obtain the best hit with the clustering radius set at 10 Å. The filtered poses were subjected to RDOCK for optimization of poses with CHARMm. This program takes the ZDOCK output file as input and creates the receptor and ligand atomic coordinates automatically for CHARMm. After the RDOCK optimization, the predicted poses were re-ranked based on the RDOCK score using the re-rank script. The lowest RDOCK energy pose was selected for further study. The ACE was used to estimate the contribution of the desolvation energy to the scoring function (Zhang et al. 1997). The ACE score of a pair of protein atoms is defined as the free energy difference between two protein atoms and water contacts and the sum of a protein–atom to protein–atom contact and a water to water contact. The desolvation energy of forming a protein complex (ΔG_{ACE}) from individual receptor and ligand structures is the sum of the atomic ACE scores of all receptor–ligand atom pairs within a distance cutoff of 6 Å. The scoring function of RDOCK is the sum of ACE desolvation energy and the CHARMm electrostatics energy (Chen et al. 2003):

$$\Delta G_{\text{binding}} = \Delta G_{\text{ACE}} + \beta \times \Delta E_{\text{elec}},$$

where β is a scaling factor, set by the user (default value: 0.9).

The protein–protein complex was also validated using automated docking server: ClusPro server, ZDOCK.

Molecular dynamics analysis

All molecular dynamics works were performed on a Silicon Graphics Octane2 computer running Irix 64 6.5, 600 MHz (SGI, 1600 Amphitheatre Parkway, Mountain View, CA 94043) using CVFF and the Discover3 molecular dynamics software module of the Insight II molecular modeling graphical interface (Molecular Simulations Inc.). The predicted dimer of the $A_{2A}R$–D_2R complex was subjected to energy minimizations followed by 10,000 steps each of conjugate gradient and steepest descent minimization, the criteria being a derivative of less than 0.01 Å. This minimized structure then underwent a 20,000 step dynamics simulation using the Discover3 dynamics software with a step size of 10 ps. The calculations were done at standard 300 K at neutral pH 7.0, with all trajectories calculated using an atom-based non-bonded parameter; a 12 Å non-bonded cut-off distance was used at a dielectric constant of 2 for solvent (Accelrys Inc. Discover3 tutorial).

Dynamic properties of $A_{2A}R$–D_2R

The slow mode structural dynamic properties were calculated in the framework of GNM (Haliloglu et al. 1997). The structural dynamic property ($C_{[\text{whole,slow}]}$) describes the strength of global stretch-contract or hinge-bending motion in the protein complexes (Bai et al. 2008). Thus, the global motion is depicted by slow modes, and $C_{[\text{whole,slow}]}$ was defined as the average correlation between slow mode motion of residues in two protomers, i.e.:

$$\begin{aligned} C_{[\text{whole,slow}]} &= \left\langle C_{ij,i\in\text{A},j\in\text{B}} \right\rangle \\ C_{ij,i\in\text{A},j\in\text{B}} &= \frac{\left\langle \Delta R_i \Delta R_j \right\rangle}{\sqrt{\left\langle \Delta R_i^2 \right\rangle \left\langle \Delta R_j^2 \right\rangle}}, \end{aligned} \tag{1}$$

where i and j denoted a residue of protein A ($A_{2A}R$) and B (D_2R), respectively, C_{ij} is the correlation between slow mode motion of residues i and j, $\langle \Delta R_i \Delta R_j \rangle$ is the equilibrium correlation between fluctuations of residue i and j in slow modes. On the other hand, $\langle \Delta R_i \Delta R_j \rangle \propto [\Gamma^{-1}]_{ij}$, where $[\Gamma^{-1}]_{ij}$ is the i and jth element of the inverse of connection matrix (or Kirchhoff matrix) Γ. (Bahar et al. 1997; Haliloglu et al. 1997)

$$\begin{aligned} C_{[\text{whole,slow}]} &= \left\langle \frac{[F^{-1}]}{\sqrt{[F^{-1}]_{ii}[F^{-1}]_{jj}}} \right\rangle \\ [F^{-1}]_{ij} &= \sum_{k\in\text{slow}} \lambda_k^{-1} u_{ik} u_{jk}, \end{aligned} \tag{2}$$

where F^{-1} is the slow mode part of Γ^{-1}, λ_k is the eigenvalue of kth mode, u_{ik} and u_{jk} are direction vectors of residues i and j in the eigenvector of kth mode. λ_k, u_{ik} and u_{jk} are obtained by diagonalizing Γ, the connection matrix.

Another structural dynamic property A_{off} was defined as the summation of amplitudes of dissociation-related modes. Here, the dissociation-related mode was defined as the correlation between motion of two protomers was smaller than −0.22 (the optimized cutoff value of $C_{[\text{whole,slow}]}$ for the classification of biological and crystal packing complexes), and is given as

$$A_{\text{off}} = \sum_{C_{\text{A:B}},K<-0.22} A_K = \sum_{C_{\text{A:B}},K<-0.22} 3K_{\text{B}}T/\gamma \times \lambda_{\text{K}}^{-1}, \tag{3}$$

where K_B is the Boltzmann constant, T is the thermodynamic temperature, γ is a uniform spring constant.

The correlation between motions of two protomers in mode k was:

$$C_{A:B,K} = \frac{1}{n_A n_B} \sum_{i \in A, j \in B} u_{ik} u_{jk}, \quad (4)$$

where n_A and n_B are number of residues in protein A and B, u_{ik} and u_{jk} are same as described in Eq. 2.

Secondary structure composition

Four parameters (Alpha, Beta, SurfAlpha, and Surf-Beta) representing compositions of secondary structures were calculated. Alpha was the percentage of residues in α-helix. Beta was the percentage of residues included in β-sheet. SurfAlpha and SurfBeta were percentages of residues included in α-helix and β-sheet at surfaces of protein–protein complexes. Alpha and Beta were calculated based on the output of DSSP program (Kabsch and Sander 1983). SurfAlpha and SurfBeta were obtained from the output of the web server ProtorP (Reynolds et al. 2009), which also uses DSSP to define secondary structures of protein complexes.

H-bond perturbations

The HBPlus program was used to analyze the perturbations of tertiary hydrogen bond resulted in conformation change of $A_{2A}R$–D_2R amino acid residues (McDonald and Thornton 1994; Bikadi et al. 2007). This algorithm consisted of two steps: firstly, it located the positions of hydrogens, and then calculated the hydrogen bonds. The interaction was counted as a hydrogen bond, if it is between a donor and acceptor atom and the angles and distances of donor and acceptor atoms lie within 4 Å. The residue versus residue HB plot was created in which the existed hydrogen bond shown as point between the residue number of X-axis and the residue number of Y-axis. The diagonal of graph represented the main chain ($C\alpha$) of protein, helices can be identified as strips directly adjacent to the diagonal, antiparallel beta strands by strips perpendicular to the diagonal, and parallel beta strands by off-diagonal strips parallel to the diagonal.

The evolutionary trace method: triplet homology

A set of 48 pairs of receptors (mainly belonging to GPCRs family) was used to study the receptor–receptor interactions, based on the mathematical model and experimental evidence, a set of triplet homologies have been identified that are responsible for PPI (Tarakanov and Fuxe 2010). Such amino acid triplets were mainly located in the experimentally confirmed receptor interfaces and consistent with protein interaction interfaces predicted by other bioinformatics methods (Agnati et al. 2010). In our study, the $A_{2A}R$–D_2R heterodimer complex and their interfacial contacts have been analyzed for the basic set of common triplets in each participating receptor that may be responsible for the receptor–receptor interaction.

Hot spots favoring aggregation

In protein small subset of interface residues, called "hot spots", account for most of the binding affinity, often binding specificity and PPIs (Clackson and Wells 1995; Moreira et al. 2007). Identifying these hot-spot residues within protein–protein interfaces can help us better to understand PPIs and may also help us to modulate protein–protein binding (Gonzalez-Ruiz and Gohlke 2006). The knowledge-based FADE and contacts (KFC) applied for the prediction of subset of residues that account for most of a protein interfaces with their binding free energy (Darnell et al. 2008). For each residue in the interface, the KFC server characterizes its local structural environment and compares that with the environments of experimentally determined hot spots and predicts if the interface residue is a hot-spot. The KFC model comprises two decision tree-based classifiers: K-FADE (based on shape specificity features calculated by the fast atomic density evaluator, or FADE) (Mitchell et al. 2001) and K-CON (based on biochemical contact features). K-FADE predicts hot spots using the size of the residue and the radial distribution of shape specificity and interface points. K-CON predicts hot spots in terms of intermolecular atomic contacts, hydrogen bonds, interface points and chemical type of amino acid residues.

Results

Molecular modeling of receptors with cytoplasmic loops

Three-dimensional structures provide valuable insight into molecular function and also enable the analysis of its interaction with suitable substrates. The crystal structure of $A_{2A}R$ lacked the structure of ICLs, and C-terminal residues ($\approx$120 amino acid residues) which were biologically essential for $A_{2A}R$–D_2R interaction study (Borroto-Escuela et al. 2010a, b). In addition, the tip of the second extracellular loop (E148–S156) was not modeled owing to weak experimental electron density. Presently, the modeling of the human $A_{2A}R$ and D_2R was carried with the recently solved GPCR crystal structures (PDB ID: 3PBL, 2RH1,

and 3EML) and $A_{2A}R$ (PMDB ID: PM0074986) consisted with all ECLs as templates (Luthra et al. 2009). These templates were aligned structurally to define SCRs and Clustal-X (2.0.11) used to define the conserved residues (Supplementary Fig. S1). The stereo-chemical quality of the modeled co-ordinates of $A_{2A}R$ and D_2R on SAVS server exhibited that 98.9 and 98.4% residues of $A_{2A}R$ and D_2R, respectively, were present in the most favored regions (A, B, L) of the Ramachandran plot (PROCHECK) and none of the residues of $A_{2A}R$ were found to be in disallowed regions, whereas only three residues (S103, I183, and S311) of D_2R were in disallowed region (Supplementary Fig. S2). However, these three residues were not involved in any interaction. The modeled 3D structure of $A_{2A}R$ characterized with seven transmembrane α-helices (7TM, helices 1–7) followed by one short membrane-associated helix (helix 8) parallel to cytoplasm interface, an extracellular amino-terminus (N terminus), a cytosolic carboxy terminus (C terminus), three extracellular loops (ECL1-3) and three intracellular loops (ICL1–3). The longest cytoplasmic loop at C-terminal of $A_{2A}R$ (310–412) consisted of small fragments of five β-sheets and two α-helix connected with loops as shown in Fig. 1 (Supplementary Table S4). Similarly, the predicted 3D model of D_2R showed true resemblance with $A_{2A}R$, which is the characteristic feature of GPCR protein. However, the longest ECL-2 connecting the TM4 and TM5, where as longest ICL3 was involved in connecting the TM5 and TM6 (Fig. 1). The ICL3 of D_2R containing 160 amino acid residues was orchestrated with small fragments of 3 β-sheets and 13 α-helix (see Supplementary Table S4). The modeled structure of $A_{2A}R$ with side chain superimposed with its crystal structure (PDB ID: 3EML) showed significantly reasonable rmsd value 0.252, to demonstrate the correctness of predicted model. The optimized co-ordinates of $A_{2A}R$ and D_2R were submitted to PMDB server. The 3D information of $A_{2A}R$ (PMDB ID: PM0077535) and D_2R (PMDB ID: PM0077536) could be accessed from (http://mi.caspur.it/PMDB).

Elucidation of $A_{2A}R$–D_2R aggregation

The optimization of structures and conformation of $A_{2A}R$, D_2R and $A_{2A}R$–D_2R complex in proximity to cellular atmosphere, MD simulation up to10 ps were performed with steepest descendent followed with conjugated gradient to achieve derivative 0.01 kcal mol^{-1} $Å^{-1}$. The relative reference frame corresponding to the optimized conformation of D_2R, $A_{2A}R$ and $A_{2A}R$–D_2R complex showed average displacement of frame for D_2R, $A_{2A}R$ and $A_{2A}R$–D_2R complex were 2.05, 5.33 and 2.09 Å, respectively (Supplementary Figs. S3a, S3b). The optimized model of $A_{2A}R$–D_2R complex showed that N-terminal (TM-I) of $A_{2A}R$ was oriented toward the C-terminal (TM-V) of D_2R, and $A_{2A}R$ (TM-VI/VII) was involved in contact with D_2R (TM-IV/V) (Fig. 1a). The ICL3 of $A_{2A}R$ containing motif 371AQE373 was in close association with ICL3 of D_2R having motif 276AQE278. $A_{2A}R$–D_2R complex showed minimum energy as compared to individual protein, indicating the stable complex formation (Supplementary Fig. S3b)

Structural comparisons and interfacial geometric properties

The pairwise 3D alignment and structural similarity (SSM) comparison of $A_{2A}R$ and D_2R, using PDBeFold (SSM) showed significant structural homology with *P* score 0.8 and *Z* score 5.7 with rmsd value 2.10, even though the sequence homology was only 35%. Interfacial geometric properties calculated using ProtorP (summarized in Supplementary Table S1). The larger interface accessible area

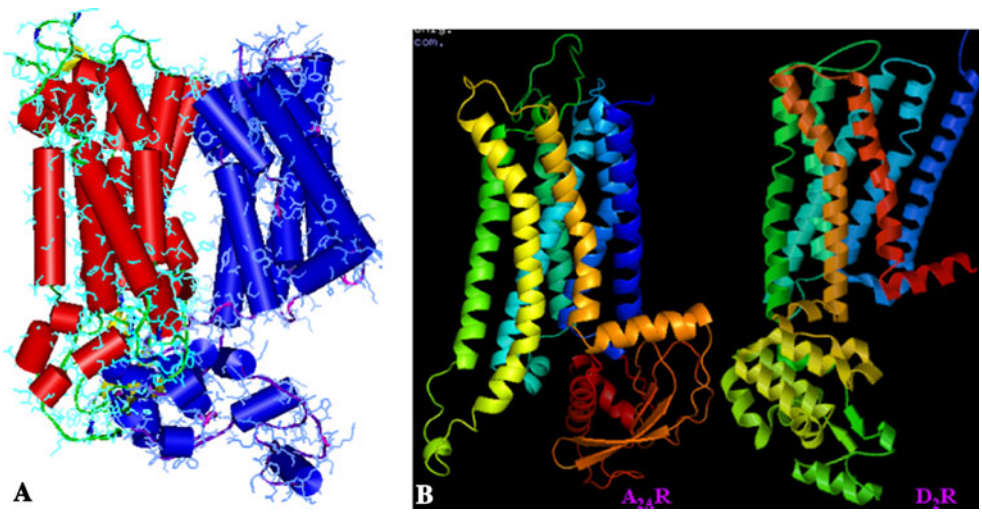

Fig. 1 **a** The Insight II view of $A_{2A}R$ (*red*)–D_2R (*blue*) docked complex. The TMs (helixes), sheets, loops and bends of $A_{2A}R$ colored with *red*, *yellow*, *green* and *blue*, respectively. D_2R, TMs (helixes), sheets, loops and bends were colored with *blue*, *marine*, *purple blue*, *purple*, respectively. **b**. Cartoon view of modeled structure of $A_{2A}R$ and D_2R (PyMol). The longest intracellular loop (ICL3) of D_2R connecting TM5 and TM6, whereas ICL3 of $A_{2A}R$ lies after TM7-helix 8 and extended up to C-terminal (color figure online)

469.23 $Å^2$ denoted interaction and consequently, formation of stable complex between the two proteins. Planarity (0.982 Å) and eccentricity (0.857) described the overall shape of interface, in which Gap was the average distance between surface of $A_{2A}R$ and D_2R.

Structural dynamic properties

The eigenvalue (λ_K) and the direction of residue vector (u_i and u_j) were calculated using GNM. The calculated spring constant (γ) values for $A_{2A}R$, D_2R and $A_{2A}R$–D_2R were 0.088, 0.048 and 0.013, respectively (Eqs. 2 and 3). The values for two structural dynamic properties ($C_{[\text{whole,slow}]}$ and A_{off}) of $A_{2A}R$–D_2R were 0.875 and −0.24, respectively. The calculated value of the correlation of dissociated mode for two promoters is −0.22 (the optimized cutoff value of $C_{[\text{whole,slow}]}$ for the classification of biological and crystal packing complexes) (Bai et al. 2008), which was closed to the found value −0.24 for $A_{2A}R$–D_2R. The calculated standard value for correlation of slow mode (association) has not been reported; however, value more than 0.5 is considered to be better for association (Bai et al. 2011). The value obtained for $A_{2A}R$–D_2R complex was 0.875 (higher than 0.5). The summation of amplitude of kinetic constant of $A_{2A}R$–D_2R, i.e., 0.635 [0.875 + (−0.24)] was significant as the value more than 0.5 has been reported as considerable value for other receptors (Bai et al. 2008) denoting stable interfacial contact between the $A_{2A}R$ and D_2R. On the basis of *B* factor and GNM calculations, the correlation coefficient of K_d and K_{on} was 0.294 showed that the physical properties of contacts have large surface area. The result showed that significant correlation value >0.5 represented the correlation between structural and kinetic parameter as well. It is true because the major interaction was present in ICL3 loops of both protomers ($A_{2A}R$ and D_2R), which were structured with helixes and sheets (Fig. 1b; Supplementary Table S4). The observed structural dynamic properties were further validated with the application of web server-based NMA and AD-ENM analysis.

The quantitative measurement of slow mode deformability

NMA normal mode analysis was performed on molecular model constructs of the D_2R–$A_{2A}R$ complex, which was used to examine the propensity of amino acid residues involved in contact formation. By comparing the spectrum of NSAD (Fig. 2), it showed that N-terminal residues, and residues from 200 to 412 residues of $A_{2A}R$ were feasible for formation of contact as these residues exhibit higher displacement than standard value 0.5 Å (Hollup et al. 2005). Similarly, higher amplitude area appearing in spectrum for D_2R showed that higher displacement of

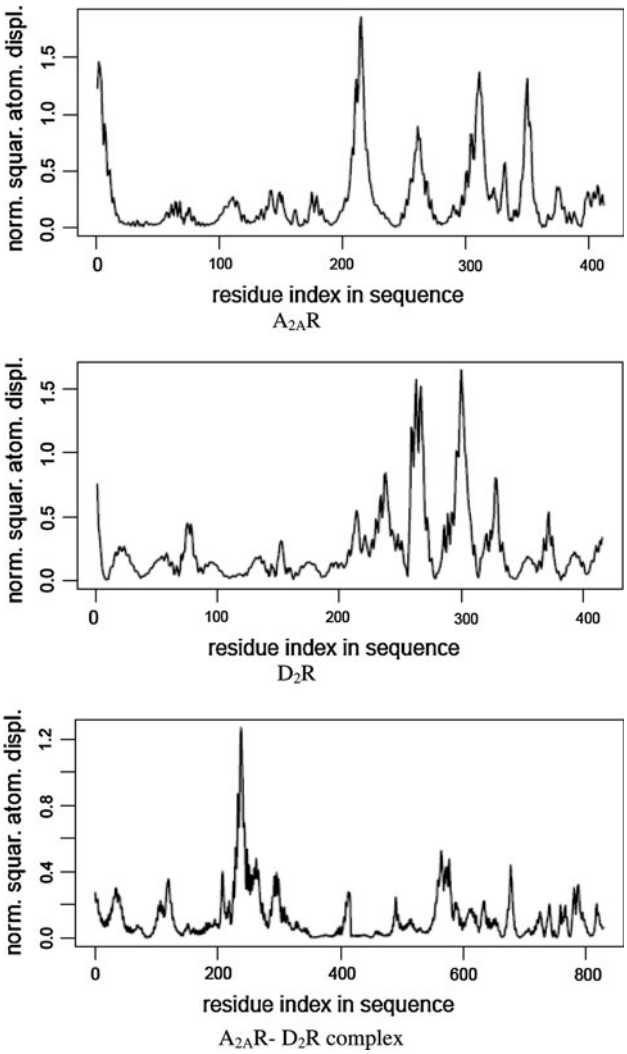

Fig. 2 The NSAD spectrum of residues in $A_{2A}R$ and D_2R interface showed that the average displacement of residues was 0.5 Å. The residues of loops regions have higher displacement than 0.5 Å. After the formation of $A_{2A}R$–D_2R complex, the average displacement of residues drops down below 0.4 Å indicating the stability of system. The average displacement of residues above 0.4 Å belonged to extracellular loops not involved in intra- and inter-protein interaction. More quantitatively the fraction of residues ($A_{2A}R$: 310–412 and D_2R: 220–370) involved in contact formation showed mobility

amino acid residues recline between approximately 250 and 350. The displacement shown for N terminus of D_2R is slightly lower, compared to C terminus, and experimental data showed that N terminus of D_2R did not participate in interaction. NSAD spectrum for D_2R–$A_{2A}R$ complex showed that D_2R (C-terminal) domains are more flattened for contact than the C terminus of $A_{2A}R$. The calculated lowest deformation energies for $A_{2A}R$, D_2R and D_2R–$A_{2A}R$ complex were 733.58, 224.57 and 555.53 kcal/mol, respectively, and showed stable complex formation of D_2R–$A_{2A}R$. The largest amplitude peaks for deformation energy denoted the movement of domain. In present study,

the predicted models of $A_{2A}R$ and D_2R showed that ICLs of both protomers participating in contact formation consisted of stable conformation (α-helixes and β-sheets). The predicted results were in agreement with recent study, suggesting ICLs of $A_{2A}R$ and D_2R were essentially participated in receptor dimerization (Borroto-Escuela et al. 2010a, b).

Classification of secondary structure of protein and deformation energy

The deformation energy for each residue is directly proportional to the sum of differences in square distance with interacting residues compared to the equilibrium state. The deformation energy profile of the first mode of $A_{2A}R$ and D_2R is shown in Fig. 3. The plot of the rmsd fluctuation per residue along the simulations revealed that residues belonging to TMs regions of $A_{2A}R$ and D_2R had almost identical fluctuations (stacked with x-axis) and showed stable conformation. However, overall energy state revealed the modest differences were visible for residues belonging to $A_{2A}R$ and D_2R. The regions of the higher variance represented the fluctuations of loops (ECLs and ICLs). Lower fluctuations of ICLs3 of $A_{2A}R$ and D_2R compared to ECLs (1–3) and ICLs (1–2) in both proteins (Fig. 3) infer that these regions were exposed to interface of $A_{2A}R$–D_2R contacts.

The mean square fluctuations of residues are obtained using the PowerB method, which also yields the correlation coefficient between $B^{\exp}$ and B^{GNM}, and the value of the effective spring constant, g. The cross-correlation map gives the normalized correlation,

$$C_{ij} = \langle \Delta R_i \Delta R_j \rangle \Big/ \left[\left\langle (\Delta R_i)^2 \right\rangle \left\langle (\Delta R_j)^2 \right\rangle \right]^{1/2},$$

between the fluctuations of residues i and j The correlations vary between -1 and 1, and they are presented by color-coded maps (Fig. 4). A value of -1 refers to a perfect anti-correlation between residue fluctuations, i.e., the motions of residues i and j are coupled but in opposite directions (colored dark blue), while $+1$ indicates the perfect concerted motion in the same direction (dark red). $C_{ij} = 0$ for uncorrelated (or perpendicular) fluctuations. Currently, cross-correlation maps are reported for submitted structures containing less than 800 nodes.

Interfacial interactions of $A_{2A}R$–D_2R dimerization

Using molecular dynamics simulations, slow mode analysis and data integrated from evolutionary trace analysis showed that the deduced set of triplets homology (AAR, AQE, VLS, and VYI) were crucial for $A_{2A}R$–D_2R heterodimer formation (Tarakanov and Fuxe 2010). The multiple sequence analysis (Supplementary Fig. S1) of the receptors ($A_{2A}R$, D_2R, D_3R and β_2R) showed that DRY motif was conserved in the four GPCR proteins. Bayesian Network-based approach predicted that the probability of the interaction of $A_{2A}R$–D_2R protein sequences with each other was 0.52867 (Jansen et al. 2003). These promising results suggested to predict the hot spots for $A_{2A}R$–D_2R dimer complex for further elucidation of interfacial interaction. Further, H-bond perturbation, salt-bridge formation, sulfur-bridge and cation–π interaction within the $A_{2A}R$,

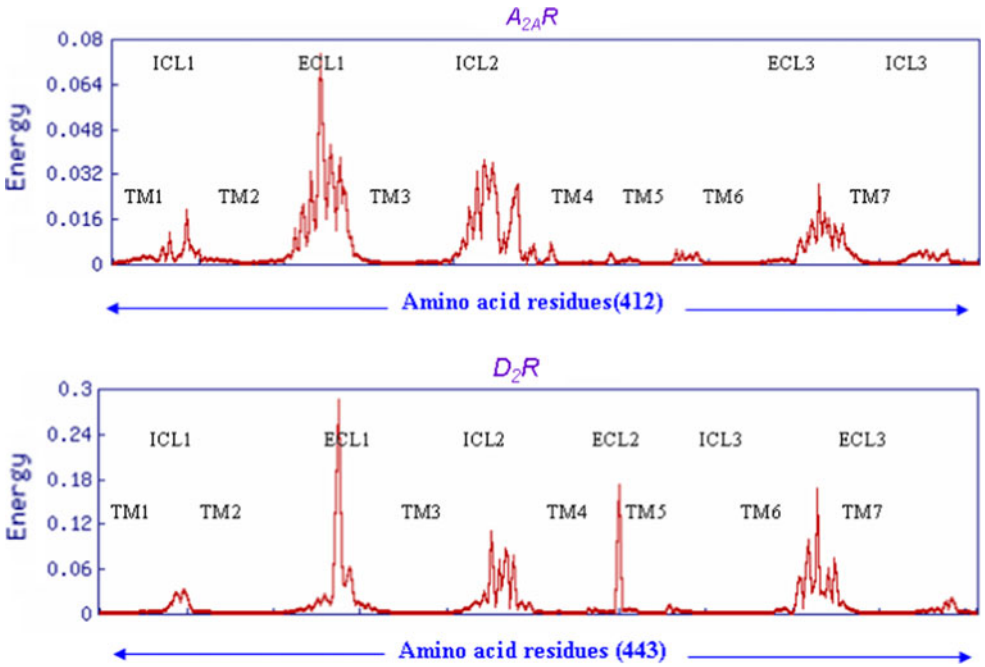

Fig. 3 Deformation energies of residues associated with the motions driven by the slowest mode of $A_{2A}R$ and D_2R in dimer complex. Stable fluctuation refers to the stable conformation of protein (TMs), more fluctuation represents the loops of protein. ICL3 of $A_{2A}R$ (amino acid residues 290–412) showed more stable conformations similarly ICL3 of D_2R (amino acid residues 214–373) showed stable conformation as TMs regions. The amino acid residues 7–13 in length connected the TM4, TM5 and TM6 of $A_{2A}R$

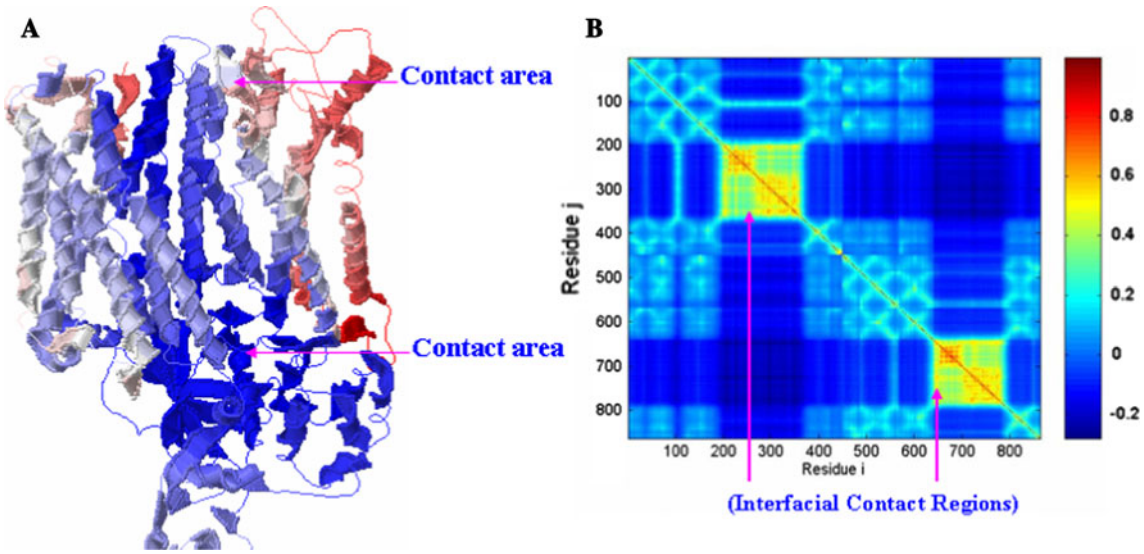

Fig. 4 **a** Color-coded ribbon diagram illustrating the mobilities in the lowest frequency GNM mode using Jmol. The structure is colored from *blue* to *red* in the order of increasing mobility. **b** Cross-correlation map of *B* factor, C_{ij}-*B*, between residue fluctuations, plotted as a function of residue indices *i* (abscissa) and *j* (ordinate). The pairs subject to fully correlated motions ($C_{ij} = +1$) are colored *dark red*; those undergoing anti-correlated motions (i.e., $C_{ij} < 0$) are colored *blue*, and moderately correlated and uncorrelated ($C_{ij} \approx 0$) regions are *yellow* and *cyan*, respectively (color figure online)

Table 1 Interaction surfaces predicted by bioinformatics and experimental findings

Receptor	Predicted location	Experimental location
$A_{2A}R$	TM1 (N-terminal), TM4, TM6, TM7, ICL3, C-terminal	TM4, TM6, ICL3, C-terminal
D_2R	TM4, TM5, TM6, ICL3, C-terminal	TM4, TM5, ICL3, C-terminal

Canals et al. (2003) and Borroto-Escuela et al. (2010a, b)

D_2R and $A_{2A}R$–D_2R complex illustrated to understand molecular basis and stability of interfacial residues.

Sequential and structural analysis of $A_{2A}R$ and D_2R

The aggregation index using AGGRESCAN (based statistical analysis of primary sequence of proteins) (Conchillo-Solé et al. 2007) suggested the roles of TM1, TM2, ECL1, TM5, TM6, TM7 of $A_{2A}R$ and TM1, TM2, TM4, TM5, TM6 of D_2R were the probable region for the formation of $A_{2A}R$–D_2R (Supplementary Table S2). However, the present study and reported BRET–FRET analysis showed the major involvement of C-terminal tails of $A_{2A}R$ and ICLs3 of D_2R in dimer interface interaction than TMs regions. The present results showed that TM1, TM6, TM7, helix-8 and ICL3 of $A_{2A}R$ and TM5, TM6 and ICL3 of D_2R were involved in interfacial contact. The involvements of TM1, TM6 and TM7 of $A_{2A}R$ and TM5, TM6 of D_2R in the formation of interfacial contacts between $A_{2A}R$ and D_2R are consistent with previous results (Agnati et al. 2010) (Table 1). This approach is based on the observation that disordered proteins are less prone to aggregation compared to structurally ordered domains of a GPCR. Although AGGRESCAN is quite powerful in identifying residues that could be functionally essential for PPI, it often does not achieve specific interaction interfaces and may provide false positive results. Consequently, other criteria (structure based) KFC (HOT-SPOT) was used.

Interfaces and hot-spot analysis

The hot-spot analysis of $A_{2A}R$–D_2R dimer complex for the prediction of residues within the protein interface showed that the hot-spot index for amino acid of N-terminal (TM1), TM6, TM7 and ECL3 (C-terminal) of $A_{2A}R$ has K-CON_{conf} values 0.72–0.81. Similarly, the K-CON_{conf} values for amino acid residues of D_2R were 0.69–0.83 involving the regions of TM4, TM5, TM6 and ICL3 (Table 2). The aggregation index for ECLs of $A_{2A}R$–D_2R dimer complex did not show significant value of confidence (i.e., <0.40) showing that these regions were not relevant for protein aggregation (Supplementary Table S2). The obtained results were consistent with recent BRET and FRET analysis of $A_{2A}R$–D_2R complex in living system

Table 2 Structural hot-spot analysis for interfacial residues of $A_{2A}R$ and D_2R

Residues of $A_{2A}R$		Residues of D_2R	
N terminus (TM1)	Y9, I10, E13	TM4	K149, R150
TM2	P61		
TM6	M174, R205	TM5	S229, L249
TM7		TM6	R361, N396
ICL3	L301, E333, R337, N348, S350, H353, E353, E355, R357, A371, Q372, E374, S374	ICL3	A276, Q277, E278, T293, R294, D320, E326, L336, M358, R360
C-terminal	D401, D402, P403, L404, D407, G408	C-terminal	R434, F437

(Borroto-Escuela et al. 2010a, b) which showed that N-terminal part of ICL3 of D_2R interacted with negatively charged C-terminal motif of $A_{2A}R$ containing two aspartate residues D401–D402 and a serine residue S374 (Tables 1, 2).

The result of ZDOCK analysis showed the interaction of N-terminal (TM1) of $A_{2A}R$ with TM5 and TM6 of D_2R, which was consistent with KFC server analysis (Fig. 1; Table 2). Earlier, it was assumed that only stable conformation of proteins was sustainable for formation of contact. However, $A_{2A}R$-predicted model suggested that ICL3 (291–412) of $A_{2A}R$ possessed small fragments of loops, bends, sheets and was rich in helix, hence participated in stable contact formation (Figs. 2, 3). Due to discrete distribution of helix, sheet and long size ($\approx$122 amino acid residues), probably the electron density map in crystallography would be weak to model this part. The ICL3 ($\approx$160 amino acid residues from 214 to 373) of D_2R

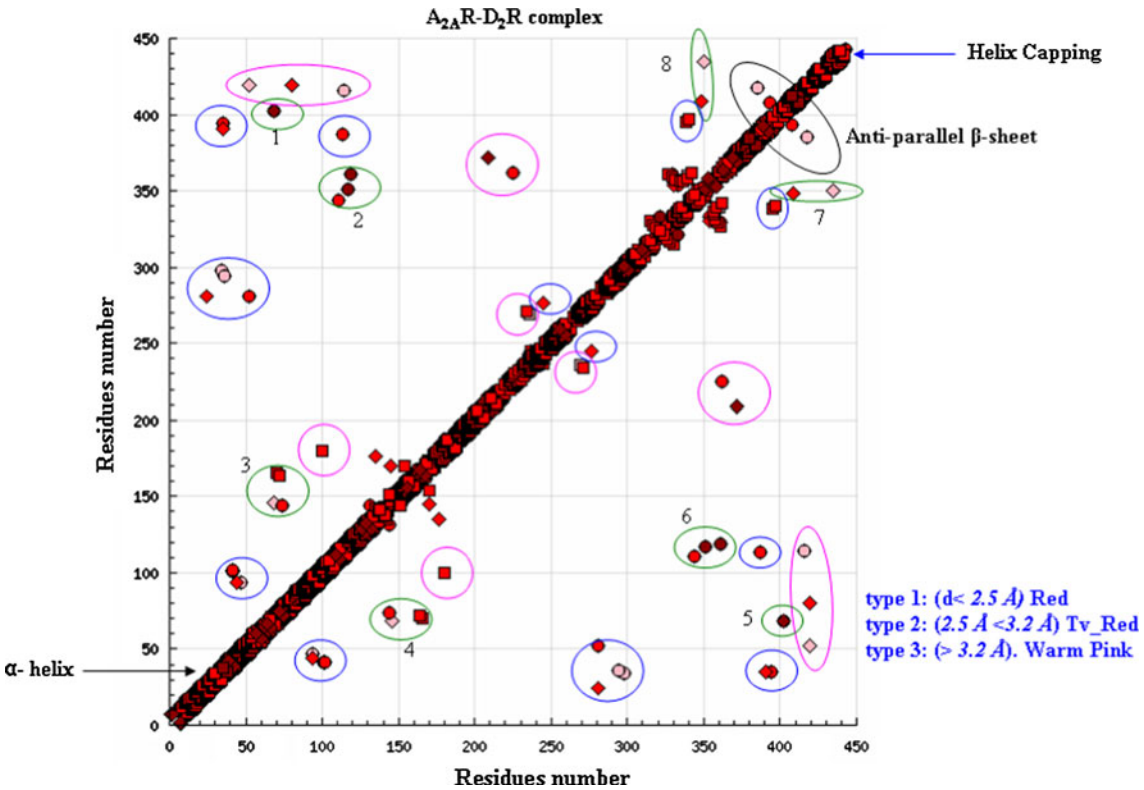

Fig. 5 HB plot representation. Helices can be identified as strips directly adjacent to the diagonal, antiparallel beta strands by strips perpendicular to the diagonal, and parallel beta strands by off-diagonal strips parallel to the diagonal. $A_{2A}R$ residues were represented as *blue circle*, D_2R residues were represented as *pink circle*, and $A_{2A}R$–D_2R interaction residues represented by *green circles*. *Circles 1* and *2* showed the N terminus ($A_{2A}R$) interaction with C terminus (D_2R) and *circle 7* represented the perturbations at C terminus of both receptor, whereas *circle 3* represented the tertiary interaction between the Pro61 of $A_{2A}R$ with Lys149 of D_2R. Tertiary interactions represented here is symmetric to diagonal. Three classes of hydrogen bondings are distinguished by color coding; namely, *red* short (distance smaller than 2.5 Å between donor and acceptor), *tv-red* intermediate (between 2.5 and 3.2 Å), and *pink* long hydrogen bonds (greater than 3.2 Å) (color figure online)

connecting the TM5 and TM6 of D_2R was also rich in helix and showed more stable conformation than $A_{2A}R$.

H-bond perturbation of $A_{2A}R$–D_2R complex

In order to illustrate the possible flow of information within the protein, residues that are in close proximity within PPI site and interfacial geometric properties of contact domain HB plot method were used to analyze the network of tertiary H-bond interactions in $A_{2A}R$, D_2R and $A_{2A}R$–D_2R complex (Supplementary material Fig. S4). Main diagonal represents the local interactions in the protein $A_{2A}R$ and D_2R, while off-diagonal points represent the tertiary interactions, and cross-diagonal arrangements represent the β-sheet. The green circles marked 1 and 2 showed TM6 of D_2R interacting with C-terminal of $A_{2A}R$ and circles 7 and 8 represented the tertiary perturbation at ICLs of both receptor (Fig. 5). The green circles, 3 and 4, showed the tertiary H-bond between the Pro 61 of $A_{2A}R$ and Lys149 D_2R. It is reasonable to assume that in order to have a prompt effect of perturbation on the whole protein, the perturbation should go through tertiary interaction points; however, no major information was obtained from H-bond perturbation except the tertiary interaction of Pro61 of $A_{2A}R$ and Lys149 D_2R. Similar finding was observed for KFC hot-spot analysis (Table 2).

Salt-bridge analysis

Salt bridge is actually a combination of two non-covalent interactions: hydrogen bonding and electrostatic interactions. This is most commonly observed to contribute stability to the entropically unfavorable folded conformation of proteins. Although non-covalent interactions are known to be fairly weak interactions, small stabilizing interactions can add up to make an important contribution to the overall stability of a conformer (Dennis 2006). The thermodynamics of each was explored through experimental procedures to assess the free energy contribution of the salt bridge to the overall free energy of the state. The results of salt bridge formed in intra-protein ($A_{2A}R$, D_2R) and inter-protein ($A_{2A}R$–D_2R complex) are summarized in Table 3. The changes in the salt bridge formation observed in ICLs region of $A_{2A}R$ and D_2R suggested that ICLs region was accessibly involved in $A_{2A}R$–D_2R dimer formation (Fig. 6; Table 3). The residues of $A_{2A}R$ forming salt bridge between E332 and H353 vanished after formation of $A_{2A}R$–D_2R complex, whereas residues E312 and K315 of D_2R formed new salt bridge after formation of $A_{2A}R$–D_2R complex shown in bold in Table 3 (Fig. 6).

Protein interaction analysis with PIC

The interactions within a protein structure and interactions between proteins in an assembly are essential considerations in understanding molecular basis of stability and functions of proteins and their complexes. Besides the H-bond and salt bridge, there are several interactions such as disulfide bonds, interactions between hydrophobic residues, ionic interactions, hydrogen bonds, aromatic–aromatic interactions, aromatic–sulfur interactions and cation–π interactions within a protein or between proteins in a complex that render stability to a protein structure or assembly. The Protein Interactions Calculator (PIC) server was used to calculate the disulfide bridges and cation–π interaction to ensure comprehensive contact analysis of

Table 3 The amino acid residue-wise chart of intra-protein and inter-protein salt bridge interaction of $A_{2A}R$, D_2R and $A_{2A}R$–D_2R complex

$A_{2A}R$ residues		Dist (Å)	D_2R residues		Dist (Å)
Intraprotein salt bridges of $A_{2A}R$ and D_2R					
D101	R102	2.76	D131	R132	3.07
K209	E212	2.75	R227	E368	3.92
E212	R220	3.66	R227	E368	3.92
E219	R222	3.20	K367	E368	3.16
E355	R337	3.24	**E312**	**K315**	**2.76**
E355	R337	3.98			
E355	R357	2.97			
E332	**H353**	**2.76**			
Residues			Dist (Å)		
Interprotein salt bridges of $A_{2A}R$ and D_2R after complex formation					
E355 ($A_{2A}R$)		R434 (D_2R)	3.73		

The residues of $A_{2A}R$ given in bold shown for salt bridge between E332 and H353 vanished after formation of $A_{2A}R$–D_2R complex, whereas residues (E312 and K315) of D_2R formed new salt bridge after formation of $A_{2A}R$–D_2R complex, shown in bold

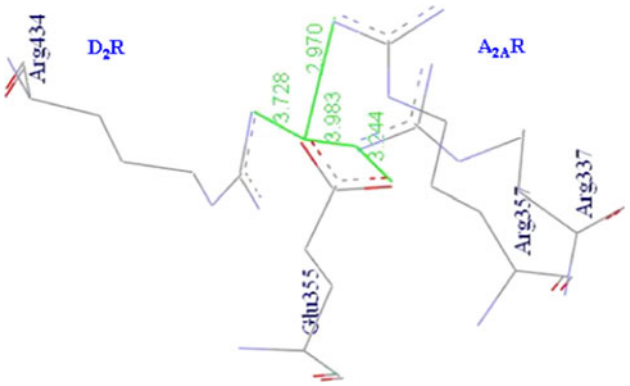

Fig. 6 Salt bridge formed (shown with *green color*) between R434 of D_2R and E355 $A_{2A}R$ at interfacial region of $A_{2A}R$–D_2R interaction (color figure online)

$A_{2A}R$–D_2R complex. The results obtained from PIC server showed that there was no significant change in disulfide bridge and cation–π interactions of $A_{2A}R$ and D_2R after formation of $A_{2A}R$–D_2R complex and ECLs regions were intact (Supplementary Table S3). This suggested that ECLs were not involved in $A_{2A}R$–D_2R complex formation; however, intact disulfide bridges and integral ECLs demonstrated the correctness of predicted models (Ivanov et al. 2009).

Discussion

Essentially, the prediction of 3D structure of $A_{2A}R$ and D_2R with ECLs and ICLs was carried to study the kinetics of $A_{2A}R$–D_2R aggregation and propensity of interfacial amino acid residues. Recently, the set of triplet sequential homologies responsible for receptor–receptor interaction has been deduced by rigorous mathematical model approach to study receptor assimilations (Block et al. 2007; Mizuno et al. 2008). Such triplet code can also be utilized to determine and predict which receptors should or should not form heterodimers at sequential level (Tarakanov and Fuxe 2010). $A_{2A}R$ and D_2R possessed triplet sequential homology AAR in the ICL3, AQE in C-terminal tail of the $A_{2A}R$ and ICL3 of D_2R supporting the important role of these intracellular domains in the heteromer interface. Instead, the triplet homology VLS is located in the TM-IV of the two protomers and the VYI in the N-terminal of $A_{2A}R$ and TM-V of D_2R indicating a role of TM-IV and TM-V in the $A_{2A}R$–D_2R receptor interfaces. Taking together with the BRET and FRET experimental results and these in silico predictions suggested the existence of a basic set of common triplets in the two participating receptors in the $A_{2A}R$–D_2R heteromers that may participate in the receptor–receptor interaction interfaces at the intracellular and transmembrane levels (Borroto-Escuela et al. 2010a, b). Present results were consistent with earlier report, and demonstrated electrostatic interactions between the C-terminal tail of $A_{2A}R$ and the ICL3 of D_2R and showed the role of the TM-IV and TM-V segments of D_2R in mediating the antagonistic $A_{2A}R$–D_2R interaction (Borroto-Escuela et al. 2010a, b). The molecular dynamic modeling also implies TM-IV of $A_{2A}R$ interacted with TM-IV/V of D_2R and TM-I/VII of $A_{2A}R$ interacted with TM-IV/V of D_2R. The models obtained also indicate the position of the pro-triplet homologies and are compatible with the theory (Tarakanov and Fuxe 2010) that the pro-triplets AAR, AQE, and VLS through guide-clasp interactions play an important role in the $A_{2A}R$–D_2R heteromer interface. The role of $A_{2A}R$ (S374, D401 and D402) lying at C-terminal in the formation of dimer, as indicted in BRET-FRET was not observed in ZDOCK and MD simulation study. However, ENM and hot-spot analysis showed that S374, D401 and D402 of $A_{2A}R$ were involved in interaction with R294, L336 of D_2R. The salt bridge interaction of E355 ($A_{2A}R$) with R434 (D_2R) provided the stability to the interfacial contact. The obtained predictions pertaining to the $A_{2A}R$–D_2R contact interfaces are in substantial agreement with experimental data of other GPCRs. The presence of potential interaction surfaces in both the intra-membrane portion of the molecules (in particular, at the level of TM4, TM5, and TM6) and in the intracellular loops (in particular, IL3 and C-terminal) is consistent with reported data (Canals et al. 2003; Guo et al. 2003). The result of kinetic study of association–dissociation of $A_{2A}R$–D_2R complex using slow mode elastic network model showed that the correlation coefficient of K_d and K_{on} was 0.294 and the correlation coefficient of K_d and K_{off} was 0.635 describe stable interfacial contact of dimer. The calculated anisotropic B factors, displacement parameters (ADPs), are found correlated. These parameters describe static disorder (atomic coordinate differences between unit cells), dynamic disorder (the diffraction data represent a time average of protein motion), rigid-body motion of the protein, internal motion of the protein. The data (Figs. 2, 3) obtained here showed that after contact formation at the interface region has lower fluctuation (maximum lies at 0.1–0.2) as compared to the sable configuration TMs of both protein $A_{2A}R$ and D_2R.

Conclusion

Precisely, the predicted 3D structure of $A_{2A}R$ and D_2R with ICLs and ECLs was used to study the $A_{2A}R$–D_2R heterodimerization. The C-terminal loops and ICLs3 of $A_{2A}R$ and D_2R proteins, respectively, consisting small fractions of helixes and β-sheets with loops and bends, form stable platform for interfacial contacts. The kinetics of

association and dissociation of $A_{2A}R$–D_2R complex in slow mode analysis followed by GNM and KFC (hot-spot)-based structural analysis correctly predicted that the interfacial residues, S374, D401, and D402 of $A_{2A}R$ were involved in coulombic interaction with R294, L336 of D_2R. In structural motif at interfaces of dimer contact (Table 2) showed that besides the H-bond and salt bridge, coulombic interaction played major role in contact formation. The predicted K_{on} and K_{off} on structure-based features (e.g., Alpha, Beta, SurfAlpha, and SurfBeta; GapIndex, Leakiness and Gap Volume) showed that the association of $A_{2A}R$–D_2R is stable at neutral pH and standard temperature 300 K. The low level of G proteins is not determined by the time course of receptor activation; the present work described the structural evidence of interfacial contacts and $A_{2A}R$–D_2R dimerization by the use of computational tools. Moreover, the dynamic structural information of the $A_{2A}R$ and D_2R interaction at interfaces could contribute to enable a step toward understanding the mechanism of signaling of purinergic receptors, and their role in pharmacological and functional implications. In addition, the study could be used as a valuable model in providing plausible insight to resolve the mechanism of PPI.

Acknowledgments Amresh Prakash is thankful to Council of Scientific and Industrial Research, Delhi, India, for providing the funds and fellowship to carry this work.

References

Accelrys Inc. (2002) Forcefield-based simulations. Accelrys, Inc., San Diego. http://www.accelrys.com/doc/life/insight2000.1/ffbs/FF_SimulTOC.html

Agnati LF, Fuxe K, Zini I et al (1980) Aspects on receptor regulation and isoreceptor identification. Med Biol 58:182–187

Agnati LF, Ferré S, Lluis C et al (2003) Molecular mechanisms and therapeutical implications of intramembrane receptor/receptor interactions among heptahelical receptors with examples from the striopallidal GABA neurons. Pharmacol Rev 55:509–550

Agnati LF, Guidolin D, Vilardaga JP, Ciruela F, Fuxe K (2010) On the expanding terminology in the GPCR field: the meaning of receptor mosaics and receptor heteromers. J Rec Signal Transduct Res 30:287–303

Bahar I, Atilgan AR, Erman B (1997) Direct evaluation of thermal fluctuations in proteins using a single-parameter harmonic potential. Fold Des 2:173–181

Bahar I, Chennubhotla C, Tobi D (2007) Intrinsic dynamics of enzymes in the unbound state and relation to allosteric regulation. Curr Opin Struct Biol 17:633–640

Bai H, Ma W, Liu S, Lai L (2008) Dynamic property is a key determinant for protein–protein interactions. Proteins 70:1323–1331

Bai H, Yang K, Yu D, Zhang C et al (2011) Predicting kinetic constants of protein–protein interactions based on structural properties. Proteins 79:720–734

Bikadi Z, Demko L, Hazai E (2007) Functional and structural characterization of a protein based on analysis of its hydrogen bonding network by hydrogen bonding plot. Arch Biochem Biophys 461:225–234

Block ML, Zecca L, Hong JS (2007) Microglia-mediated neurotoxicity: uncovering the molecular mechanisms. Nat Rev Neurosci 8:57–69

Boehr DD, Nussinov R, Wright PE (2009) The role of dynamic conformational ensembles in biomolecular recognition. Nat Chem Biol 5:789–796

Borroto-Escuela DO, Marcellino D, Narvaez M et al (2010a) A serine point mutation in the adenosine A2AR C-terminal tail reduces receptor heteromerization and allosteric modulation of the dopamine D2R. Biochem Biophys Res Commun 393:767–772

Borroto-Escuela DO, Correia PA, Perez Alea M et al (2010b) Impaired M(3) muscarinic acetylcholine receptor signal transduction through blockade of binding of multiple proteins to its third intracellular loop. Cell Physiol Biochem 25:397–408

Brooks BR, Janezic D, Karplus M (2004) Harmonic analysis of large systems: methodology. J Comput Chem 16:1522–1542. doi: 10.1002/jcc.540161209

Canals M, Marcellino D, Fanelli F et al (2003) Adenosine A2A-dopamine D2 receptor–receptor heteromerization: qualitative and quantitative assessment by fluorescence and bioluminescence energy transfer. J Biol Chem 278:46741–46749

Castrignanò T, De Meo PD, Cozzettol D et al (2005) The PMDB Protein Model Database. Nucleic Acids Res 34:306–309. doi: 10.1093/nar/gkj105

Chen R, Li L, Weng Z (2003) ZDOCK: an initial-stage protein-docking algorithm. Proteins 52:80–87

Ciruela F, Burgueño J, Casadó V et al (2004) Combining mass spectrometry and pull-down techniques for the study of receptor heteromerization. Direct epitope–epitope electrostatic interactions between adenosine A2A and dopamine D2 receptors. Anal Chem 76:5354–5363

Ciruela F, Casadó V, Rodrigues RJ et al (2006) Presynaptic control of striatal glutamatergic neurotransmission by adenosine A1–A2A receptor heteromers. J Neurosci 26:2080–2087

Clackson T, Wells JA (1995) A hot spot of binding energy in a hormone-receptor interface. Science 267:383–386

Conchillo-Solé O, de Groot NS, Avilés FX, Vendrell J, Daura X, Ventura S (2007) AGGRESCAN: a server for the prediction and evaluation of "hot spots" of aggregation in polypeptides. BMC Bioinf 8:65–70

Cui Q, Bahar I (2005) Normal mode analysis: theory and applications to biological and chemical systems (mathematical and computational biology). CRC Press, Boca Raton

Dalrymple MB, Pfleger KD, Eidne KA (2008) G protein-coupled receptor dimers: functional consequences, disease states and drug targets. Pharmacol Ther 118:359–371

Darnell SJ, LeGault L, Mitchell JC (2008) KFC server: interactive forecasting of protein interaction hot spots. Nucleic Acids Res 36:265–269

DeLano WL (2003) PyMOL reference manual. DeLano Scientific LLC, San Carlos

Dennis A (2006). Modern physical organic chemistry. University Science Books, Sausalito. ISBN: 1-891389-31-9

Eisenmesser EZ, Millet O, Labeikovsky W et al (2005) Intrinsic dynamics of an enzyme underlies catalysis. Nature 438:117–121

Engel CK, Chen L, Privé GG (2002) Insertion of carrier proteins into hydrophilic loops of the *Escherichia coli* lactose permease. Biochim Biophys Acta 1564:38–46

Eran E, Yang LW, Bahar I (2006) Anisotropic network model: systematic evaluation and a new web interface. Bioinformatics 22:2619–2627

Ferrandon S, Feinstein TN, Castro C et al (2009) Parathyroid hormone mediates sustained cyclic AMP production by

endocytosis of ligand-receptor-G protein complexes. Nat Chem Biol 5:734–742
Ferre S, Fuxe K (1992) Dopamine denervation leads to an increase in the intramembrane interaction between adenosine A2 and dopamine D2 receptors in the neostriatum. Brain Res 594:124–130
Ferre S, Snaprud P, Fuxe K (1993) Opposing actions of an adenosine A2 receptor agonist and a GTP analogue on the regulation of dopamine D2 receptors in rat neostriatal membranes. Eur J Pharmacol 244:311–315
Ferre S, Ciruela F, Canals M et al (2004) Adenosine A2A-dopamine D2 receptorreceptor heteromers. Targets for neuropsychiatric disorders. Parkinsonism Relat Disord 10:265–271
Fuxe K, Agnati LF, Benfenati F et al (1983) Evidence for the existence of receptor–receptor interactions in the central nervous system. Studies on the regulation of monoamine receptors by neuropeptides. J Neural Transm Suppl 18:165–179
Fuxe K, Ferre S, Canals M et al (2005) Adenosine A2A and dopamine D2 heteromeric receptor complexes and their function. J Mol Neurosci 26:209–220
Fuxe K, Marcellino D, Borroto-Escuela DO, Frankowska M et al (2010) The changing world of G protein-coupled receptors: from monomers to dimers and receptor mosaics with allosteric receptor–receptor interactions. J Rec Signal Transduct 30:272–283
Gonzalez-Ruiz D, Gohlke H (2006) Targeting protein–protein interactions with small molecules: challenges and perspectives for computational binding epitope detection and ligand finding. Curr Med Chem 22:2607–2625
Discover 3 User Guide (1999) MSI, San Diego
Guo W, Shi L, Javitch JA (2003) The fourth transmembrane segment forms the interface of the dopamine D2 receptor homodimer. J Biol Chem 278:4385–4388
Haliloglu T, Bahar I, Erman B (1997) Gaussian dynamics of folded proteins. Phys Rev Lett 79:3090–3093
Henzler-Wildman K, Kern D (2007) Dynamic personalities of proteins. Nature 450:964–972
Hollup SM, Salensminde G, Reuter N (2005) WEBnm@: a web application for normal mode analyses of proteins. BMC Bioinf 11(6):52
Hooft RWW, Vriend G, Sander C, Abola EE (1996) Errors in protein structures. Nature. 381:272
Ivanov AA, Palyulin VA, Zefirov NS (2007) Computer aided comparative analysis of the binding modes of the adenosine receptor agonists for all known subtypes of adenosine receptors. J Mol Graph Model 25:740–754
Ivanov AA, Barak D, Jacobson KA (2009) Evaluation of homology modeling of G-protein-coupled receptors in light of the A2A adenosine receptor crystallographic structure. J Med Chem 52:3284–3292
Jansen R, Yu H, Greenbaum D et al (2003) Bayesian networks approach for predicting protein-protein interactions from genomic data. Science 302:449–453
Kabsch W, Sander C (1983) Dictionary of protein secondary structure: pattern recognition of hydrogen-bonded and geometrical features. Biopolymers 22:2577–2637
Kim S-K, Gao Z-G, Van Rompaey P et al (2003) Modeling the adenosine receptors: comparison of the binding domains of A2A agonists and antagonists. J Med Chem 46:4847–4859
Lamb T (1996) Gain and kinetics of activation in the G-protein cascade of phototransduction. Proc Natl Acad Sci USA 93:566–570
Larkin MA, Blackshields G, Brown NP, Chenna R et al (2007) Clustal W and Clustal X version 2.0. Bioinformatics 23: 2947–2948
Laskoswki RA, MacArthur MW, Moss DS et al (1993) PROCHECK: a program to check the stereochemical quality of protein structures. J Appl Cryst 26:283–291
Lohse MJ, Nikolaev NO, Hein P et al (2008) Optical techniques to analyze real-time activation and signaling of G-protein- coupled receptors. Trends Pharmacol Sci 29:159–165
Luthra PM, Prakash A, Barodia SK et al (2009) In silico study of naphtha [1, 2-d] thiazol-2-amine with adenosine A 2A receptor and its role in antagonism of haloperidol-induced motor impairments in mice. Neurosci Lett 463:215–218
Maier-Peuschel M, Frolich N, Dees C et al (2010) A FRET-based M2 muscarinic receptor sensor reveals rapid kinetics of allosteric modulation. J Biol Chem 285:8793–8800
McDonald IK, Thornton JM (1994) Satisfying hydrogen bonding potential in proteins. J Mol Biol 1238:777–793
Mishra CB, Barodia SK, Prakash A et al (2010) Novel 8-(furan-2-yl)-3-substituted thiazolo [5,4-e][1,2,4] triazolo[1,5-c] pyrimidine-2(3H)-thione derivatives as potential adenosine A(2A) receptor antagonists. Bioorg Med Chem 18:2491–2500
Mitchell J, Kerr R, Ten-Eyck L (2001) Rapid atomic density methods for molecular shape characterization. J Mol Graph Model 19:325–330
Mizuno T, Zhang G, Takeuchi H et al (2008) Interferon-γ directly induces neurotoxicity through a neuron specific, calciumpermeable complex of IFN-γ receptor and AMPA GluR1 receptor. FASEB J 22:1797–1806
Moreira IS, Fernandes PA, Ramos MJ (2007) Hot spots—a review of the protein–protein interface determinant amino-acid residues. Proteins 68:803–812
Müller CE, Jacobson KA (2011) Recent developments in adenosine receptor ligands and their potential as novel drugs. Biochim Biophys Acta 1808:1290–1308
Mustafi D, Palczewski K (2009) Topology of class A G protein-coupled receptors: insights gained from crystal structures of rhodopsins, adrenergic and adenosine receptors. Mol Pharmacol 75:1–12
Reynolds C, Damerell D, Jones S (2009) ProtorP: a protein–protein interaction analysis server. Bioinformatics 25:413–414
Rosenbaum DM, Cherezov V, Hanson MA et al (2007) GPCR engineering yields high-resolution structural insights into beta2-adrenergic receptor function. Science 318:1266–1273
Soriano A, Ventura R, Molero A et al (2009) Adenosine A2A receptorantagonist/dopamine D2 receptor-agonist bivalent ligands as pharmacological tools to detect A2A–D2 receptor heteromers. J Med Chem 52:5590–5602
Tarakanov AO, Fuxe K (2010) Triplet puzzle: homologies of receptor heteromers. J Mol Neurosci 41:294–303
Vilardaga JP (2010) Theme and variations on kinetics of GPCR activation/deactivation. J Recept Signal Transduct Res 30:304–312
Vilardaga JP, Bünemann M, Krasel C et al (2003) Measurement of the millisecond activation switch of G protein-coupled receptors in living cells. Nat Biotechnol 21:807–812
Vilardaga JP, Bünemann M, Feinstein TN et al (2009) GPCR and G proteins: drug efficacy and activation in live cells. Mol Endocrinol 23:590–599
Vilardaga JP, Agnati LF, Fuxe K, Ciruela F (2010) G-protein-coupled receptor heteromer dynamics. J Cell Sci 123:4215–4220. doi: 10.1242/jcs.063354
Woods AS, Ciruela F, Fuxe K et al (2005) Role of electrostatic interaction in receptor–receptor heteromerization. J Mol Neurosci 26:125–132
Yang LW, Rader AJ, Liu X et al (2006) oGNM: online computation of structural dynamics using the Gaussian Network Model. Nucleic Acids Res 34:24–31
Zhang C, Vasmatzis G, Cornette JL, DeLisi C (1997) Determination of atomic desolvation energies from the structures of crystallized proteins. J Mol Biol 267:707–726